International Journal of Solids and Structures 80 (2016) 73–83

Contents lists available at ScienceDirect

International Journal of Solids and Structures

journal homepage: www.elsevier.com/locate/ijsolstr

On the relationships between cellular structure, deformation modes and electromechanical properties of piezoelectric cellular solids

Sumantu Iyer[a], Maen Alkhader[b,*], T.A. Venkatesh[c]

[a] Department of Mechanical Engineering, Stony Brook University, Stony Brook, NY, USA
[b] College of Engineering, American University of Sharjah, Sharjah, United Arab emirates
[c] Department of Materials Science and Engineering, Stony Brook University, Stony Brook, NY, USA

ARTICLE INFO

Article history:
Received 14 August 2014
Revised 18 September 2015
Available online 31 October 2015

Keywords:
Piezoelectricity
Cellular solids
Finite element analysis
Honeycombs
Topology

ABSTRACT

Piezoelectrically active cellular solids are reminiscent of passive structural cellular solids, and therefore, depending on their inner cellular architecture, their cellular ligaments can deform locally by either bending or axial stretching. Three main cellular solid structures (i.e. hexagonal, tetragonal and triangular) that exemplify bending and stretching dominated piezoelectrically active cellular solids are considered. Three-dimensional finite element models were developed to understand the relationships between cellular structure, deformation modes and their effective electromechanical properties. The principal elastic, dielectric and piezoelectric properties of piezoelectric 3-1 cellular solids are insensitive to inner structure or topology in the longitudinally poled systems and highly sensitive to structure in the transversely poled systems. The in-plane electromechanical properties are highly sensitive to cellular architecture and connectivity as well. The effective out-of-plane elastic properties for all the three cellular structures depend linearly on relative density (i.e. stretching dominated), while the dependence of the in-plane effective elastic properties is linear for triangular and tetragonal cellular structures (i.e. stretching dominated) and generally non-linear for hexagonal honeycombs (i.e. bending dominated). Amongst the longitudinally poled systems, the triangular structures exhibit the highest in-plane stiffness properties. Amongst the transversely poled systems, the tetragonal structure exhibits the best overall combination of piezoelectric figures of merit.

1. Introduction

Piezoelectrically active materials play an instrumental role in a wide range of actuating and sensing applications such as hydrophones, ultrasound and echo-cardiogram devices, wherein they undertake the critical role of converting mechanical energy (e.g., due to vibrations or static strain) to electrical energy (i.e., charge) and vice versa. Piezoelectric materials intended for sensing applications are required to ideally possess a combination of characteristics such as high piezoelectric sensitivity (i.e. the ratio of the generated electric energy to the applied mechanical energy) and low acoustic impedance. Existing monolithic piezoelectric ceramics (e.g., lead zirconate titanate (PZT), barium titanate) and polymers (e.g., PVDF) exhibit less than ideal combined characteristics; ceramics have high piezoelectric sensitivity and high acoustic impedance while piezoelectric polymers exhibit low piezoelectric sensitivity and low acoustic impedance. Only composite piezoelectric materials, including both porous piezo-composites (e.g., Alvarez-Arenas and de Espinosa, 1996; Alvarez-Arenas and Freijo, 1996; Banno, 1987; Bast and Wersing, 1989; Bowen et al., 2004; Bowen and Topolov, 2003; Chen and Wu, 2004; Dunn and Taya, 1993b; Hikita et al., 1983; Iyer and Venkatesh, 2010, 2011; Kar-Gupta and Venkatesh, 2006, 2007c; Kara et al., 2003; Mikata, 2001; Nagata et al., 1980; Piazza et al., 2005; Ramesh et al., 2005; Ting, 1985; Zhang et al., 2007) and polymer based piezo-composites (e.g., Dunn and Taya, 1993a,c; Guinovart-Díaz et al., 2001; Hossack and Hayward, 1991; Kar-Gupta and Venkatesh, 2007a,b; Newnham et al., 1978; Pettermann and Suresh, 2000; Poizat and Sester, 1999; Ramesh et al., 2006; Richard et al., 2004; Skinner et al., 1978)., show promise in providing the required combined characteristics of high piezo-sensitivity and low acoustic impedance. Available piezoelectric composites, although having played a prominent role in sensing devices, are far from demonstrating ideal combinations of high piezoelectric sensitivity and reduced acoustic impedance. In addition, promising existing piezo composites (i.e., 3-1) is limited to one directional piezo-activity, along the piezo elements axial direction. A promising approach that allow for achieving closer to ideal combinations of characteristics, multi-dimensional piezo-sensitivity and tunable piezo crystal symmetry is to tailor the microstructure of piezo-composites.

* Corresponding author. Tel.: +97165152955.
E-mail address: malkhader@aus.edu (M. Alkhader).

http://dx.doi.org/10.1016/j.ijsolstr.2015.10.024
0020-7683/

Continuing efforts along this path have put the spotlight on a promising subclass of piezo-porous composites, namely piezoelectric cellular solids (e.g., Bosse et al., 2012; Challagulla and Venkatesh, 2009, 2012; Kar-Gupta and Venkatesh, 2007a, b, 2008; Marcheselli and Venkatesh, 2008) and piezoelectric ferroelectret foams (Bauer et al., 2004; Fang et al., 2007)

Recently, piezoelectric cellular solids have attracted significant interest and several experimental (Arai et al., 1991; Haun and Newnham, 1986; Li et al., 2003; Marselli et al., 1999; Ting, 1985; Ueda et al., 2010) analytical (Banno, 1987; Bowen and Topolov, 2003; Dunn and Taya, 1993b; Dunn and Wienecke, 1997; Espinosa and Tarakci, 1977) and numerical-based (Bosse et al., 2012; Challagulla and Venkatesh, 2012; Challagulla and Venkatesh, 2013; Iyer and Venkatesh, 2010, 2011; Kar-Gupta and Venkatesh, 2006, 2007c; Marcheselli and Venkatesh, 2008) studies have been performed to understand their potential, characterize their electromechanical properties and elucidate the dependence of their macroscopic properties on their inner cellular architecture (i.e. property-microstructure coupling). These efforts confirmed that piezoelectric cellular solids can exhibit significantly enhanced combinations of electromechanical properties (i.e. higher piezoelectric sensitivity and reduced acoustic impedance) (Challagulla and Venkatesh, 2012), and have shown that electromechanical properties of cellular solids depend on: shape of the porosity (e.g. spheroidal or fiber-like), cellular interconnectivity (i.e. open vs. closed cells), aspect ratio of pore geometry and level of porosity.

Prior efforts, experimental, analytical and computational, have assessed the impact of porosity on acoustic impedance and sensitivity of piezoelectric materials. Experimental studies considered several porosity configurations, including: enclosed porosity in a piezoelectric material (i.e., 3-0 type) (Arai et al., 1991; Haun and Newnham, 1986; Li et al., 2003; Marselli et al., 1999; Ting, 1985; Ueda et al., 2010); long continuous fiber-like porosity, similar to a fiber composite (i.e., 3-1 type foam) (Bast and Wersing, 1989; Wirges et al., 2007) and open-foam like porosity (i.e., 3-3 type foam) (Lee et al., 2007; Roncari et al., 2001). Results confirmed that porosity assist in enhancing the sensitivity of piezoelectric materials.

Analytical models developed to study porous piezoelectric materials considered multiple porosity configurations (3-0 and 3-1 types), and aimed to establish predictive theories to describe the electromechanical properties of piezoelectric porous materials. These analytical models either utilized simplified geometries (Banno, 1987; Bowen and Topolov, 2003; Iyer and Venkatesh, 2014) or an Eshelby-type inclusion problem by employing a Green's function approach (Dunn and Taya, 1993b; Dunn and Wienecke, 1997). Models showed that an increase in porosity leads to an increase in the figures of merit (i.e., enhanced sensing sensitivity).

Though analytical models were useful, their predictive utility was limited as they employed simplifying assumptions (e.g., geometric), generally utilized transversely isotropic constituents and could not easily accommodate complex geometries (e.g., stochastically distributed porosity, complex 3-3, 3-0 and 3-1 geometries). To accommodate accurate details, realistic porosity configurations, material anisotropy and to study the effect of the poling direction, porosity shape and orientation, finite element based analysis proved more suitable. Efforts along this path illustrated the positive correlation between porosity, increased piezoelectric sensitivity and reduced acoustic impedance (Marcheselli and Venkatesh, 2008), and emphasized the importance of pore geometry and configuration. For instance, piezoelectric properties were found to be sensitive to porosity shape in 3-0 type foams (Iyer and Venkatesh, 2010, 2011) and porosity relative orientation to poling direction in 3-1 foams (Kar-Gupta and Venkatesh, 2006, 2007c).

The aforementioned studies of piezoelectric cellular solids highlighted the strong coupling between effective electromechanical properties and cellular architecture. As for passive cellular solids this coupling can be seen as a consequence of cellular ligaments acting as networks with admissible deformation modes (Alkhader and Vural, 2008, 2009; Evans et al., 2001; Fleck et al., 2010; Pingle et al., 2011). Theoretically, this structure-property coupling can be exploited to optimize or application-tailor piezoelectric cellular solids. However, to usefully exploit this coupling it should be understood first; in particular, geometric cellular features and associated deformation modes that strongly affect the macroscopic electromechanical properties should be identified and analyzed.

Literature from passive isotropic cellular solids suggests that one of the main issues related to structure-property coupling is the role of the dominant deformation mode (i.e., bending vs. stretching (Andrews et al., 2001; Ashby et al., 2000; Deshpande et al., 2001; Onck et al., 2001; Shi and Tong, 1995)), which in turn is influenced by nodal connectivity (i.e. the average number of ligaments connected to a vertex) and the nature of applied stresses (Alkhader and Vural, 2010; Papka and Kyriakides, 1998). For piezoelectric cellular solids, there is added complexity due to the elastic, dielectric and piezoelectric anisotropy of the cellular solids constituents, the coupled electromechanical nature of the problem, the sensitivity to the poling direction and its orientation with respect to the porosity of cellular solids. Furthermore, the relationship between deformation modes, effective electromechanical properties and geometric features such as nodal connectivity in piezoelectric cellular solids is not yet completely understood or even explored.

Hence, in this paper, we develop finite element models to characterize the effect of deformation modes (bending vs. stretching) on the complete electromechanical properties of piezoelectric active cellular solids by studying two dimensional piezoelectric cellular solids with varying cellular architectures, representative of cellular solids with bending and stretching dominant deformation modes. Representative cellular solids include perfect honeycomb (represent bending dominated cellular solids), 2D triangular structure (represent stretching dominated cellular solids) and tetragonal structure (represents cellular solids with mixed or load dependent deformation modes)

The present work has been organized as follows. Section 2 illustrates the utilized methodology and discusses the details of the developed finite element models. Results are discussed in Section 3 and principal conclusions from the present study are highlighted in Section 4.

2. Methodology

2.1. Structure of piezoelectric cellular solids

Three classes of two dimensional honeycomb-like piezoelectric cellular solids are considered (Fig. 1). These have been selected to represent cellular solids with low, moderate and high nodal connectivity, which can exhibit bending-dominated, mixed-mode, or stretching-dominated deformation characteristics, depending on the loading conditions. Nodal connectivity, α, is defined as the average number of ligaments connected at a node (vertex). The low connectivity class is represented by a hexagonal honeycomb structure ($\alpha = 3$) while the moderate connectivity class is represented by tetragonal structure ($\alpha = 4$), and the high connectivity class is represented by triangular structure ($\alpha = 6$).

From literature of passive cellular solids we infer that, low connectivity honeycombs generally deform in a bending mode under in-plane normal and shear loading conditions, while highly connected cellular structures, (with a connectivity of 6 in 2D), generally deform in a stretching mode under all loading conditions (Alkhader and Vural, 2008, 2009; Deshpande et al., 2001; Guo and Gibson, 1999). The tetragonal structures deform in a mixed-mode depending on the in-plane loading direction; when the load is aligned with ligaments it deforms in a stretching mode but when the load is not aligned with cellular ligaments (and for in-plane shear loading) tetragonal

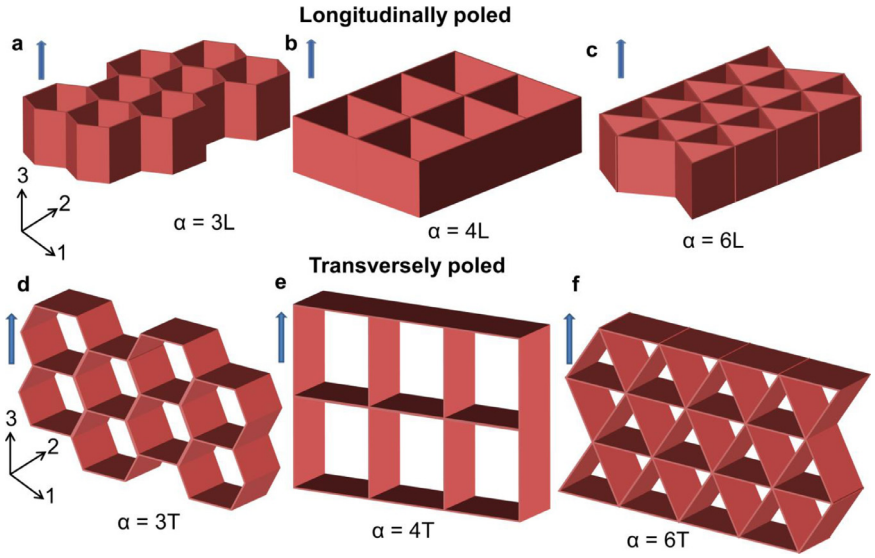

Fig. 1. Schematics illustrating the piezoelectric cellular structures with nodal connectivity (α) of 3, 4 and 6, respectively, representing honeycomb, tetragonal and triangular structures studied in the present work. In the longitudinally poled structures (a, b, c) the porosity is aligned with the poling direction (i.e. 3-direction) while in the transversely poled structures, the porosity is orthogonal to the poling direction.

Table 1
The fundamental properties of the model piezoelectric system PZT-7A (poled in the 3-direction) chosen for the present study (Density $\rho = 7700$ kg/m^3).

Properties	PZT-7A
$C_{11} = C_{22}$ (GPa)	148
C_{12} (GPa)	76.2
$C_{13} = C_{23}$ (GPa)	74.2
C_{33} (GPa)	131
$C_{44} = C_{55}$ (GPa)	25.3
C_{66} (GPa)	35.9
$e_{15} = e_{23}$ (C/m^2)	9.31
$e_{31} = e_{32}$ (C/m^2)	−2.324
e_{33} (C/m^2)	10.9
$\kappa_{11} = \kappa_{22}$ (nC/Vm)	3.98
κ_{33} (nC/Vm)	2.081

structures deform in a bending deformation mode. Therefore, one can consider the three selected classes as representatives of cellular solids that exhibit different deformation modes, which will permit the investigation of the effect of cellular solids structure (topology) and deformation modes on the effective electromechanical properties of piezoelectric cellular solids.

A model piezoelectric constituent material, PZT-7A, is chosen for the present study. The electromechanical properties of PZT-7A are presented in Table 1. The three cellular classes considered in the present work have relative densities ranging from 5% to 20%. In each of the three classes of cellular materials, longitudinally poled (i.e. poled along the porosity axis) and transversely poled (i.e. poled orthogonal to the porosity axis) systems are considered.

2.2. Constitutive behavior of piezoelectric cellular solids

The most general representation of the electromechanical coupled constitutive relationships for a piezoelectric material, in the linear elastic regime, is given by:

$$\sigma_{ij} = C^{E}_{ijkl}\varepsilon_{kl} - e_{ijk}E_k$$
$$D_i = e_{ikl}\varepsilon_{kl} + \kappa^{\varepsilon}_{ij}E_j \quad (1)$$

where *i, j, k, l* assume the value 1 to 3, $\boldsymbol{\sigma}$ and $\boldsymbol{\varepsilon}$ are the second-order stress and strain tensors respectively, **E** is the electric field vector, **D** is the electric displacement vector, $\mathbf{C}^{\mathbf{E}}$ is the fourth-order elasticity tensor with the superscript "E" indicating that the elasticity tensor corresponds to measurement of **C** at constant or zero electric field, **e** is the third-order coupling tensor, and $\boldsymbol{\kappa}^{\boldsymbol{\varepsilon}}$ is the second-order permittivity tensor measured at constant or zero strain. Eq. (1) represents the elastic, piezoelectric and dielectric coefficients and has 21 elasticity, 18 piezoelectric and 6 permittivity constants that are independent material properties. As the cellular solids studied in this work are in the elastic regime, Eq. (1) is used to represent both the cellular solids' constituent material and macroscopic response. For the latter, Eq. (1) is applied in terms of effective elastic, piezoelectric and dielectric coefficients as well as average stress and strain. Based on Eq. (1), the complete characterization of the effective electromechanical properties of piezoelectric cellular solids, in the linear elastic domain, requires identifying all 45 independent material constants.

2.3. Finite element modeling of piezoelectric cellular solids

A unit cell approach is utilized in this work; where in the electromechanical response of a large periodic piezoelectric cellular solid is characterized by modeling the behavior of a representative volume element. The finite element analysis of the unit cell is carried out using the commercial software (ABAQUS). Eight-node linear piezoelectric brick (C3D8E) elements are used to mesh the unit cell. Each node has a total of four degrees of freedom – three translational (i.e., 1, 2, 3) and one electric potential (i.e., 9 per ABAQUS convention). To ensure that the unit cell captures the response of the entire material, periodic boundary conditions are enforced. These conditions ensure that the deformation and electric potential of a unit cell are compatible across its boundaries with that of the adjacent unit cells as explained in Refs. (Iyer and Venkatesh, 2010, 2011). Periodicity is ensured by forcing parallel faces of the unit cell to remain parallel during deformation.

To apply the periodic conditions, the unit cell is modeled using a mesh that is symmetric in the 1-2, 2-3 and 1-3 planes. The periodic boundary conditions are achieved by connecting each node on one side (e.g., left) with the corresponding node on the opposite side of the unit cell (e.g., right) using constraint equations that are defined with respect to the master nodes, located on the vertices of the unit cell (Fig. 2), referred to as A, AA, B, BB, C, CC, D, and DD. Although

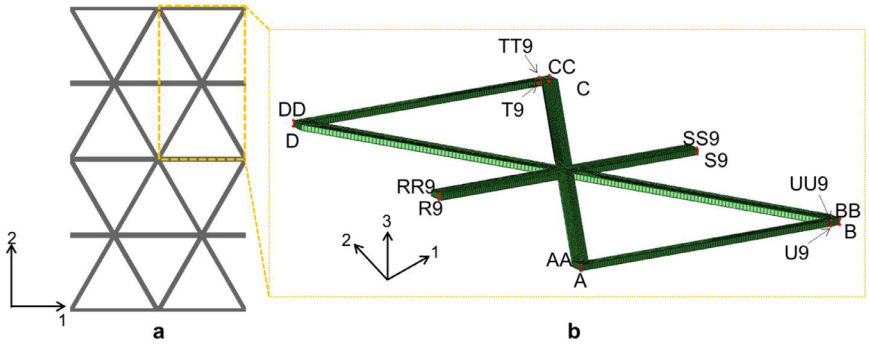

Fig. 2. (a) Schematic showing the triangular piezoelectric foam structure studied in the present work. (b) Finite element model of the corresponding unit-cell showing the master nodes and the node sets R, RR, S, SS, T, TT, U, UU located along the boundaries of the unit-cell.

Fig. 2 represents the triangular geometry, the process followed to set up the period boundary conditions is still applicable. The constraint equations are designed such that they allow the master nodes to control the overall behavior of the unit cell. All loads (mechanical and electrical) are applied to the master nodes only. The master node A is fixed and electrically grounded to prevent rigid body motion. The total number of constraint equations is almost half the number of boundary nodes in the model. To write the constraint equations in a compact form, nodes on boundary lines connecting two master nodes are assigned to a node set. Therefore, eight node sets are defined such that: R contains the nodes between A and D; RR contains nodes between AA and DD; S contains nodes between B and C; SS contains nodes between BB and CC; U contains nodes between A and B; UU contains nodes between AA and BB; T contains nodes between C and D; TT contains nodes between CC and DD. In terms of the node sets and master nodes the constraint equations are given as:

$$P^{Ri} - P^{A} = P^{Si} - P^{B};\ P^{RRi} - P^{AA} = P^{SSi} - P^{BB};\ P^{Ti} - P^{D} = P^{Ui} - P^{A};\ P^{TTi} - P^{DD} = P^{UUi} - P^{AA} \quad (2)$$

where "P" refers to the degrees of freedom (i.e., P = 1, 2, 3, and 9) and 'i' represents the node in the set, see Fig. 2.

The unit cell is subjected to a set of controlled mechanical and electrical loading conditions and its response to each loading is studied. Data from the loadings (tests) is used to determine all 45 corresponding material constants (i.e. complete electroelastic moduli: elastic, piezoelectric and dielectric). The outlined finite element modeling scheme can be adopted to determine the complete electroelastic moduli for any piezoelectric cellular architecture as long as it can be represented by a unit cell. In our prior studies, the electromechanical response of a unit-cell has also been checked to ensure that it accurately represents the electromechanical response of a larger volume of material comprised of many unit-cells (Iyer et al., 2014).

In the finite element models developed in this study, it is assumed that all regions in the piezoelectric foams are poled uniformly in one direction. From a practical point of view, such uniform poling can be readily realized in longitudinally porous honeycombs as uniform electric fields in the out-of-plane (i.e., 3) direction can be easily created in such foams. However, poling of transversely porous piezoelectric honeycombs in a uniform manner could be challenging (Iyer et al., 2014). Some regions may remain un-poled or be poled in a direction that is different from the direction that is originally intended in the poling process. However, if the porous regions were to be filled by a material with elastic modulus and dielectric constant that is considerably lower than that of the honeycomb (e.g., a polymer), then significant improvements in the uniformity of the poling characteristics across a wider region of the foams could be achieved (Iyer et al., 2014). Alternately, a poled, solid piezoelectric material may, in principle, be selectively treated such that the inner regions of the foams are removed while retaining the foam network to create a uniformly poled foam structure.

3. Results

3.1. Effective elastic properties

Using finite element analysis, for each of the three piezoelectric classes considered (see Fig. 1), the effective elastic constants represented by C^{E}_{ijkl} in Eq. (1) and the elastic moduli and Poisson's ratios were obtained. Effective constants were obtained for a range of relative densities (Fig. 3) as well as for longitudinally poled and transversely poled systems.

The finite element results for the longitudinally poled hexagonal structures were first validated using an analytical model developed for longitudinally poled porous piezo composite with circular porosity (Dunn and Taya, 1993b) (which structurally resemble the hexagonal-piezo structures considered in this work).

For the longitudinally poled systems, it is demonstrated that all the three cellular structures exhibit similar out-of-plane (i.e. 3-direction) behaviors. This outcome is anticipated as, regardless of structure (or topology), the three cellular architectures have the same projected area density, and in an out-of-plane loading scenario, the cell walls are loaded axially. However, Fig. 3 illustrates that the in-plane (i.e. 1-2 plane) behavior is highly sensitive to cellular topology and connectivity. For instance, normal effective moduli (C_{11} and C_{22}) are the lowest for the honeycomb structure and the highest for the tetragonal structure (whose ligaments, for the particular loading scenario used in this study, are aligned with loading direction). C_{11} and C_{22} for the triangular structure approach those of tetragonal structure. Coupling modulus C_{12} that defines developed stresses along the lateral direction (i.e. 2-direction) due to axial strain (i.e. 1-direction) is the highest for the honeycomb structure and the lowest for the tetragonal structure. This modulus is related to the Poisson's ratio which is sensitive to topology, particularly to inclined ligaments that couple between the two material principal directions. The most sensitive elastic property to cellular topology is the in-plane shear modulus (C_{66}), which is significantly higher for the triangular structures as compared to that of both hexagonal and tetragonal structures (Fig. 3).

However, for the transversely poled systems, the normal elastic modulus along the 2-direction is the least sensitive to the cellular topology as the three structures have the same projected area density along the 2-direction and upon loading along the 2-direction the cell walls of all the three structures are loaded axially. On the other hand, the shear modulus in the 1-3 plane (i.e. C_{55}) is the most sensitive to the foam topology with the foam structure with the highest nodal connectivity (i.e. the triangular structure) exhibiting the highest C_{55} modulus.

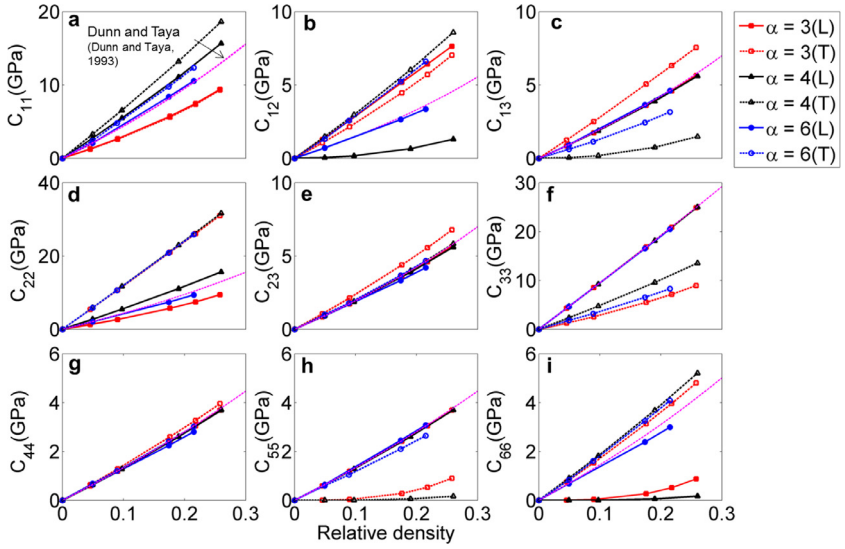

Fig. 3. Variation of the effective stiffness elastic constants with relative density in the longitudinally poled (L) and transversely poled (T) honeycomb, tetragonal and triangular piezoelectric foams structures, respectively, with nodal connectivity $\alpha = 3, 4, 6$. (The analytical model predictions by Dunn and Taya, (1993) are for a longitudinally poled system with circular porosity.)

Overall, Fig. 3 illustrates that the effective out-of-plane elastic properties (i.e. along 3-direction for longitudinally poled systems and along the 2-direction for transversely poled systems), for all the three cellular structures, are insensitive to the geometry of the foam and depend linearly on relative density. On the other hand, the dependency of the in-plane effective elastic properties (i.e. in the 1-2 plane for longitudinally poled systems and in the 1-3 plane for transversely poled systems) on relative density exhibit dependence on the cellular structure. Such that, this dependence is linear for triangular and tetragonal cellular structures (where the deformation is stretching dominated) and generally non-linear for hexagonal honeycombs (where the deformation is bending dominated). This observation is consistent with passive cellular solids literature, which illustrates that for a stretching- or bending-dominated deformation, the corresponding elastic properties, respectively, vary linearly or non-linearly with relative density.

3.2. Effective piezoelectric properties

Using finite element models, the effective piezoelectric constants represented by e_{ijk} in Eq. (1) were obtained for the three classes of cellular structures shown in Fig. 1 for a range of relative densities (Fig. 4). For each of the three classes, the corresponding piezoelectric properties of longitudinally poled and transversely poled systems were also obtained. For the 2D cellular solids considered, the non-zero effective piezoelectric properties are e_{15}, e_{24}, e_{33}, e_{31} and e_{32}. In general, the piezoelectric properties of longitudinally poled 2D cellular structures are independent of the structure or topology (Fig. 4). However, significant dependence of the piezoelectric properties on the cellular topology is observed in the transversely poled systems.

With respect to the variation of effective piezo properties with relative density, the triangular and tetragonal topologies exhibit generally linear dependence, while the hexagonal topology exhibits

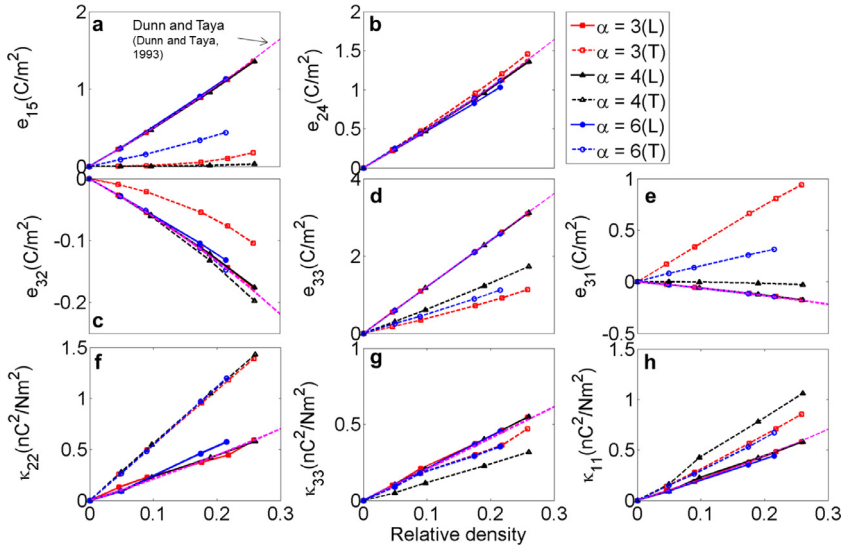

Fig. 4. Variation of the effective piezoelectric and dielectric constants with relative density in the longitudinally poled (L) and transversely poled (T) honeycomb, tetragonal and triangular piezoelectric foams structures, respectively, with nodal connectivity $\alpha = 3, 4, 6$. The analytical model predictions by Dunn and Taya, (1993) are for a longitudinally poled system with circular porosity.

non-linear dependence. This non-linear dependence is associated with shear/bending deformation related piezoelectric properties.

Amongst the transversely poled structures, the highest and the lowest e_{33} and e_{32} piezoelectric constants are observed, respectively, in the case of tetragonal and hexagonal structures. On the other hand, the piezoelectric constant e_{31} is highest for the hexagonal structure and lowest for the tetragonal structure while the piezoelectric constant e_{15} is highest for the triangular structure and lowest for the tetragonal structure. Thus, cellular structure or topology can be tailored to optimize a set of piezoelectric constants that are desired for a particular application.

3.3. Effective dielectric properties

The effective piezoelectric constants represented by $\kappa_{ij}^{\varepsilon}$ in Eq. (1) were obtained for the three cellular structure shown in Fig. 1, for a range of relative densities (Fig. 4) and for longitudinally poled and transversely poled systems. In general, the dielectric constants - κ_{11}, κ_{22}, and κ_{33}, of longitudinally poled structures and the dielectric constant κ_{22} of the transversely poled structures are independent of the cellular topology (Fig. 4). However, the dielectric constants - κ_{11} and κ_{33} of the transversely poled structures exhibit significant dependence on cellular topology. Amongst the transversely poled structures, the tetragonal foams exhibit the highest κ_{11} and the lowest κ_{33} dielectric constants while the triangular and honeycomb cellular structures exhibit relatively similar effective dielectric properties that are 10% off those exhibited by tetragonal structures.

3.4. Effective figures of merit

The aforementioned fundamental material constants are represented in this section via the industry adopted figures of merit. These figures are defined as combinations of the fundamental material constants and are used to assess the utility of piezoelectric materials for applications. Four figures of merit are of interest to piezoelectric cellular solids and their potential applications (e.g., ultrasound imagers and energy harvesters); they are: the piezoelectric charge coefficient (d_h), the hydrostatic figure of merit ($d_h g_h$), the acoustic impedance (Z), and the coupling constant (k_t) (Kar-Gupta and Venkatesh, 2006). These figures were computed using the effective fundamental material constants (elastic, piezoelectric and dielectric) presented in Figs. 3, and 4 and the results are plotted in Fig. 5 against relative density. In general, the figures of merit of longitudinally poled structures are independent of the cellular topology (Fig. 1). However, significant dependence of the figures of merit on the cellular topology is observed in the transversely poled structures which is expected, as the figures of merit are mostly dependent on the principal material elastic, piezoelectric and dielectric constants (i.e. C_{33}, e_{33} and κ_{33}) which have been shown to exhibit sensitivity to the cellular topology (in the transversely poled structures).

Amongst the longitudinally poled systems, the triangular structures with the $\alpha = 6$ exhibit figures of merit which are similar to other cellular structures as well as outstanding in-plane shear properties which are significantly better than those of the tetragonal or hexagonal structures.

Overall, the transversely poled systems exhibit better figures of merit (Z, d_h and $d_h g_h$) than the longitudinally poled systems. Amongst the investigated transversely poled systems, the tetragonal structure with a moderate level of nodal connectivity of 4, exhibits the best overall combination of high piezoelectric coupling constant, piezoelectric charge coefficient and the hydrostatic figure of merit with marginally higher acoustic impedance

Thus, by modifying the cellular topology and the poling characteristics of piezoelectric cellular structures, their mechanical and functional properties can be application tailored and optimized.

3.5. Scaling laws

Dependence of cellular solids' effective properties on relative density is often represented by scaling laws (e.g.,(Gibson and Ashby, 1997)), which are mathematical fits that generally follows,

$$\frac{E^*}{E_s} = c\,(\bar{\rho})^n = c\left(\frac{\rho^*}{\rho_s}\right)^n \tag{3}$$

where c and n are fitting parameters, E^* and E_s represent the effective property of the cellular solid and constituent material, respectively. In addition, $\bar{\rho}$ is the relative density which is defined as the ratio of the density of the cellular solid ($\rho*$) to the density to the constituent material (ρ_s). Scaling laws are useful from an application perspective as they: allow for predicting the effective properties of cellular solids over a continuous range of relative densities based on few discrete data points, assist in approximating the effective properties of cellular solid as long as they are used across cellular solid with fairly similar cellular architectures and constituent materials, and provide some insight into the deformation mechanisms. For instance, as illustrated in reference (Gibson and Ashby, 1997), as the power n increases when Eq. (3) is applied to Shear or Young's moduli, bending deformation is dominant and as it approaches unity, stretching deformation is dominant.

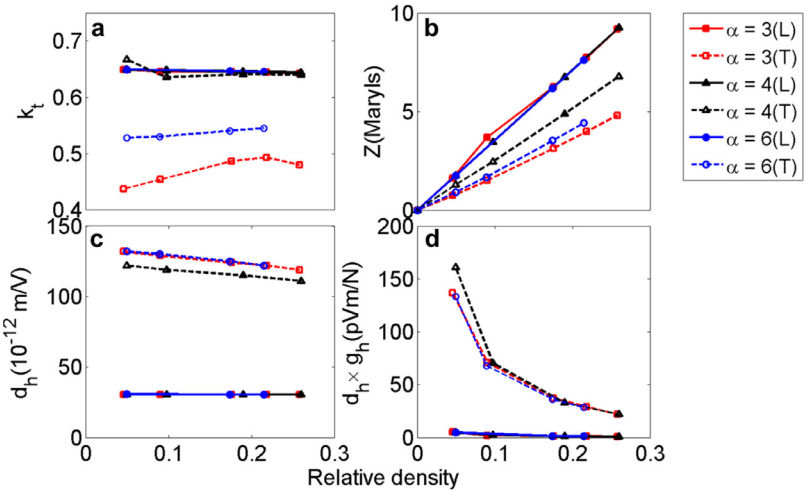

Fig. 5. Variation of the effective piezoelectric figures of merit with relative density (0.05–0.25) in the longitudinally poled (L) and transversely poled (T) honeycomb, tetragonal and triangular piezoelectric foams structures, respectively, with nodal connectivity $\alpha = 3, 4, 6$.

Table 2
The variation with relative density of the effective electromechanical properties of longitudinally poled piezoelectric foams with honeycomb, tetragonal and triangular structures captured by the scaling laws, with the corresponding coefficients a and n as described by Gibson and Ashby (1997) (C^*, e^* and κ^* represent foam properties while C, e and κ represent the properties of the constituent solid material).

Properties	Honeycomb		Tetragonal		Triangular	
	a	n	a	n	a	n
$C_{11}*/C_{11}$	0.3212	1.207	0.4429	1.065	0.3915	1.107
$C_{12}*/C_{12}$	0.4053	1.03	0.3097	2.156	0.2277	1.072
$C_{13}*/C_{13}$	0.3442	1.121	0.3381	1.116	0.3354	1.098
$C_{22}*/C_{22}$	0.3216	1.208	0.4429	1.065	0.3081	1.034
$C_{23}*/C_{23}$	0.3444	1.121	0.3381	1.116	0.2806	1.044
$C_{33}*/C_{33}$	0.7496	1.015	0.7515	1.017	0.7379	1.009
$C_{44}*/C_{44}$	0.6229	1.075	0.6159	1.072	0.5248	1.014
$C_{55}*/C_{55}$	0.6229	1.075	0.6159	1.072	0.6321	1.072
$C_{66}*/C_{66}$	1.528	3.058	0.3597	3.212	0.3947	1.014
$e_{15}*/e_{15}$	0.6229	1.075	0.6159	1.072	0.6321	1.072
$e_{24}*/e_{24}$	0.6229	1.075	0.6159	1.072	0.5248	1.014
$e_{31}*/e_{31}$	0.3442	1.121	0.3381	1.116	0.3354	1.098
$e_{32}*/e_{32}$	0.3444	1.121	0.3381	1.116	0.2806	1.044
$e_{33}*/e_{33}$	1.091	0.9944	1.099	0.9978	1.095	0.9968
$\kappa_{11}*/\kappa_{11}$	0.6232	1.075	0.5903	1.036	0.565	1.061
$\kappa_{22}*/\kappa_{22}$	0.481	0.9115	0.5903	1.036	0.2484	0.3903
$\kappa_{33}*/\kappa_{33}$	0.9523	0.9552	1.02	1.001	1.008	0.9953

For the piezoelectric cellular specimens considered in this work, all effective data presented in Figs. 3 and 4 were fitted to the scaling law (Eq. (3)). Resulting fitting constants are reported in Tables 2 and 3. Quality of the fits were ensured by visual inspection as well as by computing the R^2 regression value for each fit, which were for all fits greater than 0.96. The in-plane shear properties of the honeycomb structures (i.e., C_{66} in the longitudinally poled system and C_{55} in the transversely poled system) vary with relative density in a non-linear manner (i.e. n = 3) indicating that the in-plane shear behavior is bending dominated and hence, the in-plane moduli are expected to be less than that of tetragonal or triangular structures where the corresponding shear moduli vary with relative density in a linear manner (i.e. n = 1) indicating that the in-plane shear behavior is stretching dominated. The out-of-plane normal properties (i.e. C_{33} in the longitudinally systems and C_{22} in the transversely poled systems) for the three foam structures exhibit linear variation with relative density (i.e. n = 1) indicating that their out-of-plane normal behavior is stretching dominated.

Table 3
The variation with relative density of the effective electromechanical properties of transversely poled piezoelectric foams with honeycomb, tetragonal and triangular structures captured by the scaling laws, with the corresponding coefficients a and n as described by Gibson and Ashby (1997) (C^*, e^* and κ^* represent foam properties while C, e and κ represent the properties of the constituent solid material).

Properties	Honeycomb		Tetragonal		Triangular	
	a	n	a	n	a	n
$C_{11}*/C_{11}$	0.3286	1.231	0.5245	1.062	0.4445	1.091
$C_{12}*/C_{12}$	0.4203	1.047	0.3602	2.152	0.2353	1.124
$C_{13}*/C_{13}$	0.4223	1.129	0.4793	1.078	0.4522	1.079
$C_{22}*/C_{22}$	0.3388	1.192	0.4339	1.068	0.3178	1.055
$C_{23}*/C_{23}$	0.402	1.098	0.3628	1.139	0.321	1.067
$C_{33}*/C_{33}$	0.8254	1.012	0.837	1.013	0.8248	1.009
$C_{44}*/C_{44}$	0.6625	1.07	0.6225	1.076	0.5729	1.025
$C_{55}*/C_{55}$	0.5779	1.084	0.6098	1.069	0.5887	1.07
$C_{66}*/C_{66}$	2.219	3.052	0.5023	3.219	0.5031	1.029
$e_{16}*/e_{16}$	1.236	3.091	0.2252	3.159	0.2645	1.134
$e_{21}*/e_{21}$	−1.523	0.9733	0.2646	2.32	−0.5407	−0.9093
$e_{22}*/e_{22}$	0.4677	1.123	0.6595	1.06	0.495	1.031
$e_{23}*/e_{23}$	0.3637	1.56	0.4201	1.193	0.3648	1.154
$e_{34}*/e_{34}$	0.6626	1.07	0.6225	1.076	0.5729	1.025
$\kappa_{11}*/\kappa_{11}$	0.899	1.06	1.052	1.015	0.8381	1.048
$\kappa_{22}*/\kappa_{22}$	0.7561	0.9269	0.6523	1.077	0.4135	0.5346
$\kappa_{33}*/\kappa_{33}$	1.315	0.9787	1.347	0.981	1.482	1.035

4. Discussion and summary

The piezoelectric cellular solids analyzed in this work represent three distinct classes of cellular solids in terms of dominant deformation modes. Hexagonal structures represent bending dominated cellular solids while the triangular structures represent stretching dominated cellular solids. Finally, tetragonal structures represent cellular solids whose dominant deformation mode is dependent on the loading scenario. This classification is based on Maxwell's stability criterion which, in the field of cellular solids, has been utilized to give insight into why passive foams and honeycombs are almost always bending dominated (Deshpande et al., 2001).

Maxwell's rule as explained in (Deshpande et al., 2001; Pellegrino and Calladine, 1986) defines the condition for a pin-jointed frame made up of b struts and j frictionless joints to be both statically and kinematically determinate. This condition in 2D is written as $M = b - 2j + 3 = s - m$, where s and m counts the number of states of self-stress (i.e. redundant members exist) and of mechanisms (i.e. zero stiffness modes), respectively, and they can be determined by finding the rank of the equilibrium matrix that describes the frame in a full structural analysis (Pellegrino and Calladine, 1986). Using Maxwell's criterion, Deshpande et al. (Deshpande et al., 2001) analytically showed that the necessary and sufficient condition for rigidity of 2D periodic trusses with similarly situated nodes is a connectivity, α, of 6 such that α is the average number of struts per node. Accordingly, a pin-jointed triangular structure with a connectivity (α) of 6 is rigid, while pin-jointed tetragonal ($\alpha = 4$) and hexagonal ($\alpha = 3$) frames exhibit three and one mechanisms, respectively. Therefore, pin-jointed hexagonal frame will collapse under normal and shear loadings, while pin-jointed tetragonal frames collapse only under shear.

Structures analyzed in this work are derived from the pin-jointed frames analyzed above by locking their joints (i.e. the joints are not allowed to rotate and can transmit moment). The effect of locking the joints can be easily anticipated. As the pin-jointed triangular frame is a truss whose struts are two-point members, locking its joints will not have significant effects; at most it would give rise to negligible bending stresses in few struts. Conversely, locking the joints of the pin-jointed hexagonal frame has a significant effect; it will eliminate the three mechanisms, allow the frame to exhibit axial and shear stiffness and encourage the frame's struts to deform mostly by bending, regardless of the loading scenario. Finally, locking the joints of the pin-jointed tetragonal structure would affect its response under pure axial loading (along the 1 or 2 directions); however, it would eliminate its shear-type single mechanism and allow the tetragonal frame to provide shear stiffness by promoting bending deformations in the struts. Accordingly, the pin-jointed tetragonal structure with locked joints exhibits a response that depends on the loading scenario; its struts are loaded axially under macroscopic axial loading (in the 1 and 2 direction) and by bending under macroscopic shear loading (in the 1-2 plane).

Each of the piezoelectric cellular structures analyzed in this work can be derived from one of the idealized pin-jointed frames with locked joints discussed above. Therefore, the analysis of rigidity in the idealized pin-jointed frames, as summarized above, can give valuable insight regarding the mechanical behavior of the piezoelectric cellular structures. The triangular piezoelectric structure is derived from a rigid pin-jointed frame and should deform predominantly by cell wall stretching. On the other hand, the hexagonal piezoelectric structure is derived from a pin-jointed frame with three mechanisms and should be bending dominated. Therefore, the triangular specimen should be mechanically stiffer in the in-plane (i.e. 1-2 plane), which agrees with the finite element results. Finally, the tetragonal piezoelectric

Table 4
Analysis of the bending and axial stresses developed across the foam struts at representative locations L1 and L2 in the honeycomb, tetragonal and triangular foams with 20% relative density when subjected to six uniform (normal and shear) macroscopic strain loading conditions, which are used to determine the corresponding six fundamental elastic properties C_{ij}. The N metric is evaluated using the formula, N = 1- (Bending stress / Axial Stress). The strains applied are maintained within the linear elastic limit to approximately 0.25% for all loading conditions.

	Honeycomb (L1)			Honeycomb (L2)		
Property, loading condition	Bending stress (Pa)	Axial stress (Pa)	N	Bending stress (Pa)	Axial stress (Pa)	N
C_{11}, ε_{11}	2.35E + 04	2.81E + 06	0.992	1.36E + 06	2.65E + 06	0.487
C_{22}, ε_{22}	1.35E + 04	3.67E + 04	0.631	1.15E + 06	2.34E + 06	0.508
C_{33}, ε_{33}	1.80E + 00	1.86E + 04	1.00	5.01E + 04	3.30E + 06	0.985
C_{44}, γ_{23}	1.30E − 07	1.04E − 03	1.00	1.68E − 02	3.75E − 01	0.955
C_{55}, γ_{13}	8.50E − 05	1.35E + 00	1.00	1.58E − 02	1.44E − 01	0.890
C_{66}, γ_{23}	1.83E + 06	3.00E + 01	−60900.0	2.33E + 08	7.14E + 07	−2.26
	Tetragonal (L1)			Tetragonal (L2)		
Property, loading condition	Bending Stress (Pa)	Axial Stress (Pa)	N	Bending Stress (Pa)	Axial Stress (Pa)	N
C_{11}, ε_{11}	7.82E + 04	4.61E + 06	0.983	4.59E + 04	2.26E + 05	0.797
C_{22}, ε_{22}	4.76E + 04	2.58E + 05	0.816	0.00E + 00	3.90E + 06	1.00
C_{33}, ε_{33}	1.05E + 05	5.26E + 06	0.980	1.41E + 04	3.40E + 06	0.996
C_{44}, γ_{23}	3.19E − 05	1.33E − 03	0.976	7.54E − 02	4.38E + 00	0.983
C_{55}, γ_{13}	6.44E − 03	1.27E + 00	0.995	1.03E − 02	1.01E − 02	−0.0155
C_{66}, γ_{23}	2.29E + 04	2.50E − 01	−91600.0	2.17E + 06	7.16E + 04	−2.93
	Triangular (L1)			Triangular (L2)		
Property, loading condition	Bending Stress (Pa)	Axial Stress (Pa)	N	Bending Stress (Pa)	Axial Stress (Pa)	N
C_{11}, ε_{11}	5.14E + 05	1.57E + 07	0.967	1.40E + 06	4.30E + 06	0.675
C_{22}, ε_{22}	1.76E + 04	2.43E + 05	0.928	7.48E + 05	6.91E + 06	0.892
C_{33}, ε_{33}	5.78E + 05	1.67E + 07	0.965	5.90E + 03	1.68E + 07	1.00
C_{44}, γ_{23}	1.23E − 04	1.68E − 03	0.927	3.28E − 03	1.23E + 00	0.997
C_{55}, γ_{13}	3.18E − 02	1.95E + 00	0.984	2.96E − 03	1.49E + 00	0.998
C_{66}, γ_{23}	1.06E + 06	2.50E + 03	−425.0	2.55E + 05	4.17E + 06	0.939

structure is derived from the tetragonal pin-jointed frame; therefore it should exhibit axial deformation under uniaxial loading and bending deformation under shear loading. This agrees well with the finite element results which show that the tetragonal specimen has effective elastic and piezoelectric properties that approach those of the triangular specimen under uniaxial loading and approach those of the hexagonal specimen under shear loading (see Figs. 3 and 4).

To confirm that the dominant deformation modes exhibited by the simulated piezoelectric specimens follow the preceding theoretical arguments, stresses developed in the struts of the piezoelectric specimens were extracted and used to determine the dominant deformation mode as outlined in Ref. (Alkhader and Vural, 2009). As the deformation is elastic and struts' stiffness is uniform, stresses in struts can be decomposed using simple mechanics of materials approach into a uniform axial stress and a bending stress that varies linearly along the strut's thickness. Subsequently, the level of axial and bending stresses are used to deduce the dominate deformation mode.

For the triangular structures, stress decomposition analysis and stress contours demonstrate that, for in-plane uniaxial loading conditions (i.e. 1-2 plane in longitudinally poled systems); the struts are loaded by mostly axial stresses. Under in-plane shear loading (i.e. 1-2 plane in longitudinally poled systems) two thirds of the struts (inclined struts) are observed to be loaded axially while the straight struts are dominated by bending. However, the maximum bending stress in the horizontal struts is less than 25% of the axial stress observed in the inclined struts. For the tetragonal specimens, stress contours show that under axial loading the struts are under pure axial loading. On the other hand, for shear loading, the struts mostly exhibit bending-type deformation with the maximum bending occurring near the vertices where maximum bending stresses are more than three orders of magnitude more than the axial stresses. Finally, for honeycombs under all loading directions, stress contours showed significant bending deformation with the maximum occurring near vertices. Alkhader and Vural, (2009) showed using finite element analysis that around 20% of the elastic energy stored in a honeycomb is in the form of stretching energy.

Furthermore, the difference in the axial and bending stresses normalized by the axial stress can be used as a metric to gauge the extent of axial vs. bending deformations and predict stiffness level (i.e. high vs. low) when the structures are subjected to uniform macroscopic deformation modes (e.g. ε_{11} uniaxial strain, γ_{66} pure shear strain). When this metric is close to or equal to one, then predominant mode of deformation is expected to be stretching. As bending stresses increase, this metric proportionally decreases (Table 4). In this table, axial and bending stresses were found at the force transition points under maximum stresses (referred to as L_1 and L_2 in Fig. 6). According to the metric (Table 4), we expect the four-noded tetragonal structure to deform mostly by stretching when loaded uniaxially in the in-plane direction (i.e. 1 and 2 direction in longitudinally poled systems) as the observed metric is the highest. Consequently, we expect the corresponding elastic moduli (i.e. C_{11} or E_{11} and C_{22} or E_{22}) to be the highest for the four-noded foam structure. Similarly, the six-noded triangular structure is expected to deform mostly by stretching under in-plane shear loading (i.e. 1-2 plane in longitudinally poled systems) as the corresponding metric is the highest. Consequently, we expect the corresponding in-plane shear modulus (i.e. C_{66} or G_{12}) to be the highest for the six-noded triangular structure as well. These predictions on the elastic moduli based on the analysis of bending and axial stresses are consistent with the trends observed in the finite element analysis (Fig. 3).

One should be careful in extending results from this work to other piezoelectrically active cellular solids, since the pin-jointed frame analysis performed, assumes that the pin-jointed structure is large, periodic and has self-situated nodes. Piezoelectric cellular solids with finite, random or non-periodic structures can still be derived from parent pin-jointed structures, but the necessary and sufficient condition of rigidity for these structures might not be 6 in 2D. Instead, the rigidity analysis can be used in a general perspective to provide insight into the mechanical behavior of these piezoelectric cellular

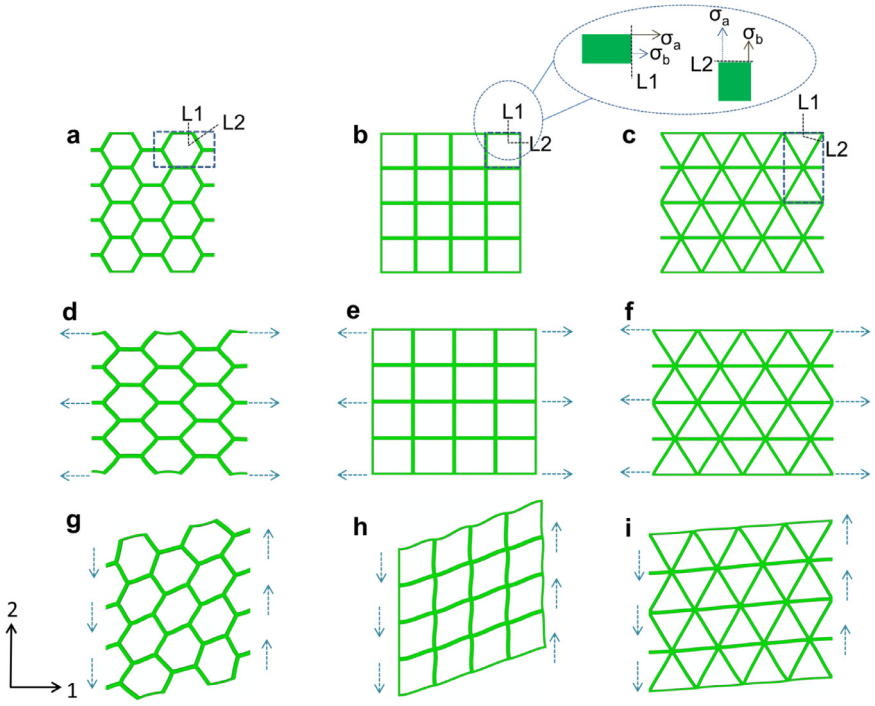

Fig. 6. The longitudinally poled honeycomb (a), tetragonal (b) and triangular (c) piezoelectric foam structures subjected to in-plane axial (d, e, f) and shear loading (g, h, i) exhibit varying degrees of bending and axial deformations. The extent of bending and axial deformation is captured by analyzing the maximum (σ_a) and minimum (σ_b) stresses developed in the foam struts at two representative cross-sections L1 and L2.

solids. To illustrate, the degree of rigidity of these structures can be related to the number of independent collapse mechanisms (m) in their parent pin-jointed frames through average connectivity α. Then, in general, as the average nodal connectivity increases, the number of collapse mechanisms in the parent structure decreases and the structure shifts toward being stretching dominated. This trend continues until the connectivity satisfies the rigidity condition, beyond which an increase in connectivity increases the number of states of self-stress and has little effect on the effective mechanical properties.

An interesting phenomenon that is worth highlighting is the ability of cellular structures or topology to affect the crystal symmetry of a piezoelectric cellular solid. For instance, although the parent material used has negative e_{31}, the triangular piezoelectric specimen exhibited a positive effective e_{31} (see Fig. 4). This reversal in sign is caused mainly by the contribution of the inclined struts to the surface charge along the 2-direction due to a load along the 1-direction. To illustrate, Fig. 7 shows the surface charge distribution observed on the top of surface of the triangular specimen due to uniaxial strain along the 1-direction. This figure shows that near the vertices, where the inclined ligaments are contributing, the charge distribution is positive,

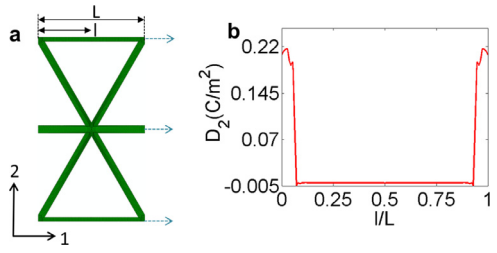

Fig. 7. (a) Schematic illustrating a unit cell that corresponds to the triangular piezoelectric foam structure subjected to a uni-axial strain along the 1-direction, where l is the position of the nodes and L is the total length of the face perpendicular to the 2-direction. (b) Figure presenting the variation of the electric displacement along the nodes on the face perpendicular to the 2-direction.

while the rest of the top surface is exhibiting close to null distribution (very small positive value).

The aforementioned results and discussion assume specific idealized assumptions that one should be aware of as they may affect the properties and the range of applicability of the piezoelectric cellular solids that have been considered in this study. For instance, properties of these piezoelectric cellular solids will highly depend on their poling characteristics, i.e., poling direction and poling uniformity. From a practical perspective realizing uniform poling, especially for the transversely poled materials, is quite challenging as the electric field passing through a porous medium tends to realign itself with the solid phase. Increasing the uniformity of the electric field distribution can, in principle, be achieved by poling the cellular structure in an oil bath with dielectric properties approaching those of the constituents of the piezo cellular solid. Such an oil bath can be created possibly by introducing dielectric particles in the oil (Iyer et al., 2014). However, 100% uniform poling may not be achieved. In such a case, it could be expected that the overall properties of piezoelectric cellular solids may deviate from the values reported here for the ideal (i.e. uniformly poled) case.

Analogous to the uniform poling assumption, the implemented model assumes uniform microstructure and grain size. Variability in the grain size would affect the overall piezoelectric properties as electromechanical properties for many piezoelectric constituents depend on grain size (Kar-Gupta and Venkatesh, 2008). In addition, it is implicitly assumed in the model developed in this study that the thickness of ligaments is larger than the grain size. Thus, grain size can limit the achievable relative density, but this might not be an issue as piezoelectric materials with 1 μm grain size are feasible (Huan et al., 2013).

It should be noted that the topology, ligament length scale and its thickness can greatly affect the range of applicability of piezoelectric cellular solids. Porous and cellular solids often exhibit dispersive characteristics and frequency band gaps that depend on the topology and length scales of the cellular architecture. However, for cellular solids with cell size on the order of 1 mm, they start to exhibit

dispersion characteristics at frequencies exceeding the acoustic range (i.e. early ultrasound) (Alkhader et al., 2015; Gonella and Ruzzene, 2008). Thus results presented here should not be generalized without a detailed investigation of piezo transducers designed to detect MHz and GHz frequencies.

Finally, the presented model is for infinitely periodic materials (far away from the boundaries). Near the boundaries and depending on the application, cellular cells can exhibit properties that deviate from the ones representing the infinitely periodic case. For instance, such scenario could stem from adhesives or other substances penetrating the boundary cells. Such device specific changes in the local structure and composition of the piezoelectric cellular solids and their influence on the effective performance characteristics of these materials need to be carefully examined with appropriate modifications to the models presented in this study.

5. Conclusions

Active piezoelectric cellular solids are a novel class of materials that have been recently proven to exhibit unique electromechanical properties. Within the context of piezoelectric cellular solids one of the most significant issues related to structure-property coupling is the role of the dominant deformation mode (i.e., bending vs. stretching), which in turn is influenced by a number of factors, much of which are yet to be fully understood, such as: nodal connectivity, the nature of stresses applied, the inherent elastic, dielectric and piezoelectric anisotropy of the constituent material, the poling direction and its orientation with respect to the porosity of cellular solids. Hence, finite element models were developed to characterize the effect of deformation modes (bending vs. stretching) on the complete electromechanical properties of two dimensional honeycomb-like piezoelectric active cellular solids. By studying piezoelectric cellular solids with varying cellular architectures, representative of cellular solids with bending and stretching dominant deformation modes, the following principal conclusions were obtained.

(1) The principal elastic, dielectric and piezoelectric properties (such as C_{33}, κ_{33} and e_{33}) of piezoelectric cellular solids are insensitive to structure or topology in the longitudinally poled systems. However, the principal electromechanical properties (i.e. C_{33}, κ_{33} and e_{33}) are strongly influenced by the cellular structure in the transversely poled systems.
(2) The in-plane (i.e. 1-2 plane for longitudinally poled systems and the 1-3 for transversely poled systems) behavior is very sensitive to cellular structure and connectivity. The highest in-plane elastic moduli (C_{11} and C_{22} in the longitudinally poled systems and C_{11} and C_{33} in the transversely poled systems) are obtained in the four-noded tetragonal foams while the highest in-plane shear moduli (i.e. C_{66} for the longitudinally poled system and C_{55} for the transversely poled system) are obtained in the six-noded triangular cellular structures.
(3) The effective out-of-plane elastic properties (i.e. along 3-direction for longitudinally poled systems and along the 2-direction for transversely poled systems), for all the three cellular structures depend linearly on relative density. On the other hand, the dependence of the in-plane effective elastic properties (i.e. in the 1-2 plane for longitudinally poled systems and in the 1-3 plane for transversely poled systems) is linear for triangular and tetragonal cellular structures and generally non-linear for hexagonal honeycombs.
(4) The linear variation of electromechanical properties of piezoelectric cellular solids with relative density is generally associated with a stretching mode of deformation while the non-linear variation is associated with relatively more bending mode of deformation. Thus, the piezoelectric cellular solid can exhibit enhanced stiffness or enhanced compliance in different directions depending on the deformation mode (respectively, stretching or bending) which in-turn is influenced by nodal connectivity and the nature of stress that is applied. For example, the six-noded triangular structure exhibit outstanding in-plane shear modulus as the dominant mode of deformation under in-plane shear loading is stretching.
(5) Scaling laws that can assist in predicting the effective electromechanical properties of piezoelectric cellular solids have been identified through fitting process. The coefficients of the scaling laws that were obtained further indicate that the triangular structures deform predominantly by axial stretching.
(6) Amongst the longitudinally poled systems, the triangular structures with the highest nodal connectivity of six exhibit outstanding in-plane shear properties which are significantly better than those of the tetragonal or hexagonal structures. However, in terms of figures of merit (acoustic impedance, piezoelectric charge coefficient, hydrostatic figure of merit and piezoelectric coupling constant) the triangular structures did not exhibit enhanced behavior.
(7) Overall, the transversely poled systems exhibit better figures of merit (acoustic impedance, piezoelectric charge coefficient and hydrostatic figure of merit) than the longitudinally poled systems. Amongst the transversely poled systems, the tetragonal structure with a moderate level of nodal connectivity of four exhibits the best overall combination of high piezoelectric coupling constant, piezoelectric charge coefficient and the hydrostatic figure of merit with a marginally higher acoustic impedance as compared to that of the hexagonal or triangular structures.
(8) Results confirm that cellular structure or topology can be tailored to optimize a set of piezoelectric constants that are desired for a particular application.

References

Alkhader, M., Iyer, S., Shi, W., Venkatesh, T., 2015. Low frequency acoustic characteristics of periodic honeycomb cellular cores: the effect of relative density and strain fields. Compos. Struct. 133, 77–84.
Alkhader, M., Vural, M., 2008. Mechanical response of cellular solids: Role of cellular topology and microstructural irregularity. Int. J. Eng. Sci. 46, 1035–1051.
Alkhader, M., Vural, M., 2009. The partition of elastic strain energy in solid foams and lattice structures. Acta Mater. 57, 2429–2439.
Alkhader, M., Vural, M., 2010. A plasticity model for pressure-dependent anisotropic cellular solids. Int. J. Plast. 26, 1591–1605.
Alvarez-Arenas, T.E.G., de Espinosa, F.M., 1996. Highly coupled dielectric behavior of porous ceramics embedding a polymer. Appl. Phys. Letters 68, 263–265.
Alvarez-Arenas, T.E.G., Freijo, F.M.d.E., 1996. New constitutive relations for piezoelectric composites and porous piezoelectric ceramics. J. Acoust. Soc. Am. 100, 3104–3114.
Andrews, E.W., Gioux, G., Onck, P., Gibson, L.J., 2001. Size effects in ductile cellular solids. Part II: experimental results. Int. J. Mech. Sci. 43 701–713.
Arai, T., Ayusawa, K., Sato, H., Miyata, T., Kawamura, K., Kobayashi, K., 1991. Properties of hydrophone with porous piezoelectric ceramics. Jpn. J. Appl. Phys. 1 30, 2253–2255.
Ashby, M.F., Evans, T., Fleck, N., Hutchinson, J.W., Wadley, H.N.G., 2000. Metal Foams: A Design Guide. BUTTERWORTH-HEINEMANN.
Banno, H., 1987. Effects of shape and volume fraction of closed pores on dielectric, elastic, and electromechanical properties of dielectric and piezoelectric ceramics - a theoretical approach. Am. Ceram. Soc. Bull. 66, 1332–1337.
Bast, U., Wersing, W., 1989. The influence of internal voids with 3–1 connectivity on the properties of piezoelectric ceramics prepared by a new planar process. Ferroelectrics 94, 229–242.
Bauer, S., Gerhard-Multhaupt, R., Sessler, G.M., 2004. Ferroelectrets: soft electroactive foams for transducers. Phys. Today 57, 37–43.
Bosse, P.W., Challagulla, K.S., Venkatesh, T., 2012. Effects of foam shape and porosity aspect ratio on the electromechanical properties of 3-3 piezoelectric foams. Acta Mater. 6464–6475.
Bowen, C., Perry, A., Lewis, A., Kara, H., 2004. Processing and properties of porous piezoelectric materials with high hydrostatic figures of merit. J. Eur. Ceram. Soc. 24, 541–545.
Bowen, C., Topolov, V.Y., 2003. Piezoelectric sensitivity of PbTiO3-based ceramic/polymer composites with 0–3 and 3–3 connectivity. Acta Mater. 51, 4965–4976.
Challagulla, K., Venkatesh, T., 2009. Electromechanical response of 2-2 layered piezoelectric composites: a micromechanical model based on the asymptotic homogenization method. Philos. Mag. 89, 1197–1222.

Challagulla, K., Venkatesh, T., 2012. Electromechanical response of piezoelectric foams. Acta Mater. 60, 2111–2127.
Challagulla, K.S., Venkatesh, T.A., 2013. Computational modeling of piezoelectric foams. JOM 65, 256–266.
Chen, Y.-C., Wu, S., 2004. Piezoelectric composites with 3-3 connectivity by injecting polymer for hydrostatic sensors. Ceram. Int. 30, 69–74.
Deshpande, V.S., Ashby, M.F., Fleck, N.A., 2001. Foam topology: bending versus stretching dominated architectures. Acta Mater. 49, 1035–1040.
Dunn, M.L., Taya, M., 1993a. An analysis of piezoelectric composite materials containing ellipsoidal inhomogeneities. Proc. Royal Soc. London. Series A: Math. Phys. Sci. 443, 265–287.
Dunn, M.L., Taya, M., 1993b. Electromechanical properties of porous piezoelectric ceramics. J. Am. Ceram. Soc. 76, 1697–1706.
Dunn, M.L., Taya, M., 1993c. Micromechanics predictions of the effective electroelastic moduli of piezoelectric composites. Int. J. Solids Struct. 30, 161–175.
Dunn, M.L., Wienecke, H.A., 1997. Inclusions and inhomogeneities in transversely isotropic piezoelectric solids. Int. J. Solids Struct. 34, 3571–3582.
Espinosa, G.P., Tarakci, U., 1977. High stability piezoelectric ceramics for resonator and saw applications. IEEE Trans. Son. Ultrason. 24, 145.
Evans, A.G., Hutchinson, J.W., Fleck, N.A., Ashby, M.F., Wadley, H.N.G., 2001. The topological design of multifunctional cellular metals. Prog. Mater. Sci. 46, 309–327.
Fang, P., Wegener, M., Wirges, W., Gerhard, R., Zirkel, L., 2007. Cellular polyethylene-naphthalate ferroelectrets: Foaming in supercritical carbon dioxide, structural and electrical preparation, and resulting piezoelectricity. Appl. Phys. Lett. 90, 192908.
Fleck, N.A., Deshpande, V.S., Ashby, M.F., 2010. Micro-architectured materials: past, present and future. Proc. Royal Soc. Math. Phys. Eng. Sci. 466, 2495–2516.
Gibson, L.J., Ashby, M.F., 1997. Cellular solids: structure and properties, 2nd Edition Cambridge University Press. ISBN: 9780521499118.
Gonella, S., Ruzzene, M., 2008. Analysis of in-plane wave propagation in hexagonal and re-entrant lattices. J. Sound Vib. 312, 125–139.
Guinovart-Díaz, R., Bravo-Castillero, J., Rodríguez-Ramos, R., Sabina, F.J., Martínez-Rosado, R., 2001. Overall properties of piezocomposite materials 1–3. Mater. Lett. 48, 93–98.
Guo, X.E., Gibson, L.J., 1999. Behavior of intact and damaged honeycombs: a finite element study. Int. J. Mech. Sci. 41, 85–105.
Haun, M.J., Newnham, R.E., 1986. An experimental and theoretical study of 1–3 AND 1-3-0 piezoelectric PZT-Polymer composites for hydrophone applications. Ferroelectrics 68, 123–139.
Hikita, K., Yamada, K., Nishioka, M., Ono, M., 1983. Piezoelectric properties of the porous PZT and the porous PZT composite with silicone rubber. Ferroelectrics 49, 265–272.
Hossack, J.A., Hayward, G., 1991. Finite-element analysis of 1-3 composite transducers. Ultrason. Ferroelectr. Freq. Control, IEEE Trans. 38, 618–629.
Huan, Y., Wang, X., Fang, J., Li, L., 2013. Grain size effects on piezoelectric properties and domain structure of batio3 ceramics prepared by two-step sintering. J. Am. Ceram. Soc. 96, 3369–3371.
Iyer, S., Alkhader, M., Venkatesh, T., 2014. Electromechanical response of piezoelectric honeycomb foam structures. J. Am. Ceram. Soc. 97, 826–834.
Iyer, S., Venkatesh, T.A., 2010. Electromechanical response of porous piezoelectric materials: Effects of porosity connectivity. Appl. Phys. Lett. 97, 072904.
Iyer, S., Venkatesh, T.A., 2011. Electromechanical response of (3-0) porous piezoelectric materials: Effects of porosity shape. J. Appl. Phys. 110, 034109.
Iyer, S., Venkatesh, T.A., 2014. Electromechanical response of (3-0,3-1) particulate, fibrous, and porous piezoelectric composites with anisotropic constituents: A model based on the homogenization method. Int. J. Solids Struct. 51, 1221–1234.
Kar-Gupta, R., Venkatesh, T., 2007a. Electromechanical response of 1–3 piezoelectric composites: A numerical model to assess the effects of fiber distribution. Acta Mater. 55, 1275–1292.
Kar-Gupta, R., Venkatesh, T., 2007b. Electromechanical response of 1–3 piezoelectric composites: an analytical model. Acta Mater. 55, 1093–1108.
Kar-Gupta, R., Venkatesh, T., 2008. Electromechanical response of piezoelectric composites: effects of geometric connectivity and grain size. Acta Mater. 56, 3810–3823.
Kar-Gupta, R., Venkatesh, T.A., 2006. Electromechanical response of porous piezoelectric materials. Acta Mater. 54, 4063–4078.
Kar-Gupta, R., Venkatesh, T.A., 2007. Electromechanical response of porous piezoelectric materials: effects of porosity distribution. Appl. Phys. Lett. 91, 062904.
Kara, H., Ramesh, R., Stevens, R., Bowen, C.R., 2003. Porous PZT ceramics for receiving transducers. Ultrason. Ferroelectr. Freq. Control, IEEE Trans. 50, 289–296.
Lee, S.H., Jun, S.H., Kim, H.E., Koh, Y.H., 2007. Fabrication of porous PZT-PZN piezoelectric ceramics with high hydrostatic figure of merits using camphene-based freeze casting. J. Am. Ceram. Soc. 90, 2807–2813.
Li, J.F., Takagi, K., Ono, M., Pan, W., Watanabe, R., Almajid, A., Taya, M., 2003. Fabrication and evaluation of porous piezoelectric ceramics and porosity-graded piezoelectric actuators. J. Am. Ceram. Soc. 86, 1094–1098.
Marcheselli, C., Venkatesh, T.A., 2008. Electromechanical response of 1-3 piezoelectric composites with hollow fibers. Appl. Phys. Lett. 93, 022903.
Marselli, S., Pavia, V., Galassi, C., Roncari, E., Craciun, F., Guidarelli, G., 1999. Porous piezoelectric ceramic hydrophone. J. Acoust. Soc. Am. 106, 733–738.
Mikata, Y., 2001. Explicit determination of piezoelectric Eshelby tensors for a spheroidal inclusion. Int. J. Solids Struct. 38, 7045–7063.
Nagata, K., Igarashi, H., Okazaki, K., Bradt, R.C., 1980. Properties of an interconnected porous Pb (Zr, Ti) O3 ceramic. Jpn. J. Appl. Phys. 19, L37–L40.
Newnham, R., Skinner, D., Cross, L., 1978. Connectivity and piezoelectric-pyroelectric composites. Mater. Res. Bull. 13, 525–536.
Onck, P.R., Andrews, E.W., Gibson, L.J., 2001. Size effects in ductile cellular solids. Part I: modeling. Int. J. Mech. Sci. 43, 681–699.
Papka, S.D., Kyriakides, S., 1998. In-plane crushing of a polycarbonate honeycomb. Int. J. Solids Struct. 35, 239–267.
Pellegrino, S., Calladine, C.R., 1986. Matrix analysis of statically and kinematically indeterminate frameworks. Int. J. Solids Struct. 22, 409–428.
Pettermann, H.E., Suresh, S., 2000. A comprehensive unit cell model: a study of coupled effects in piezoelectric 1–3 composites. Int. J. Solids Struct. 37, 5447–5464.
Piazza, D., Capiani, C., Galassi, C., 2005. Piezoceramic material with anisotropic graded porosity. J. Eur. Ceram. Soc. 25, 3075–3078.
Pingle, S.M., Fleck, N.A., Deshpande, V.S., Wadley, H.N.G., 2011. Collapse mechanism maps for a hollow pyramidal lattice. Proc. Royal Soc. Math. Phys. Eng. Sci. 467, 985–1011.
Poizat, C., Sester, M., 1999. Effective properties of composites with embedded piezoelectric fibres. Comput. Mater. Sci. 16, 89–97.
Ramesh, R., Kara, H., Bowen, C., 2005. Finite element modelling of dense and porous piezoceramic disc hydrophones. Ultrasonics 43, 173–181.
Ramesh, R., Prasad, C.D., Kumar, T., Gavane, L., Vishnubhatla, R., 2006. Experimental and finite element modelling studies on single-layer and multi-layer 1–3 piezocomposite transducers. Ultrasonics 44, 341–349.
Richard, C., Lee, H.S., Guyomar, D., 2004. Thermo-mechanical stress effect on 1–3 piezocomposite power transducer performance. Ultrasonics 42, 417–424.
Roncari, E., Galassi, C., Craciun, F., Capiani, C., Piancastelli, A., 2001. A microstructural study of porous piezoelectric ceramics obtained by different methods. J. Eur. Ceram. Soc. 21, 409–417.
Shi, G.Y., Tong, P., 1995. Equivalent transverse-shear stiffness of honeycomb-cores. Int. J. Solids Struct. 32, 1383–1393.
Skinner, D., Newnham, R., Cross, L., 1978. Flexible composite transducers. Mater. Res. Bull. 13, 599–607.
Ting, R.Y., 1985. Piezoelectric properties of a porous PZT ceramic. Ferroelectrics 65, 11–20.
Ueda, J., Secord, T.W., Asada, H.H., 2010. Large effective-strain piezoelectric actuators using nested cellular architecture with exponential strain amplification mechanisms. Mechatron. IEEE/ASME Trans. 15, 770–782.
Wirges, W., Wegener, M., Voronina, O., Zirkel, L., Gerhard-Multhaupt, R., 2007. Optimized preparation of elastically soft, highly piezoelectric, cellular ferroelectrets from nonvoided poly(ethylene terephthalate) films. Adv. Funct. Mater. 17, 324–329.
Zhang, H., Li, J.-F., Zhang, B.-P., 2007. Microstructure and electrical properties of porous PZT ceramics derived from different pore-forming agents. Acta Mater. 55, 171–181.